Frequency dependence dielectrophoresis technique for bridging graphene nanoribbons

Wahyu Waskito Aji[1], Yuki Usami[1,2,*], Hadiyawarman[1,2], Rikuto Oyabu[1], Hirofumi Tanaka[1,2,*]

[1]*Graduate School of Life Science and Systems Engineering, Kyushu Institute of Technology (Kyutech), 2-4 Hibikino, Wakamatsu, Kitakyushu 808-0196, Japan*
[2]*Research Center for Neuromorphic AI Hardware, Kyushu Institute of Technology (Kyutech), 2-4 Hibikino, Wakamatsu, Kitakyushu 808-0196, Japan*

E-mail: usami@brain.kyutech.ac.jp, tanaka@brain.kyutech.ac.jp

We attempted to bridge the unzipped GNRs and separate them from the excess SWNTs using the frequency-dependent dielectrophoresis (DEP) method by varying the frequency and applied voltage for future assembly. The atomic force microscopy image and Raman spectra proved that unzipped GNRs were successfully bridged by the DEP method at frequencies higher than 13 MHz. The theoretical calculation also supported only GNRs could be trapped from a mixture of GNRs/SWNTs suspension.

In the past few decades, numerous studies on nanoscale materials for future electronics have been carried out. Nanoscale electrical wiring is one of the biggest challenges for exceeding Moore's law owing to the limitations of fine processing technology in CMOS.[1-4] Graphene nanoribbons (GNRs), which are stripe-shaped single-atomic layer graphite, have been widely investigated owing to their high electronic mobility, strong mechanical endurance, and high flexibility.[5,6] The electrical properties of GNRs are strongly dependent on the width[7]. When GNRs are more than 10 nm in width they exhibit semimetallic behavior. On the other hand, when GNRs are less than 10 nm in width, they exhibit semiconductive behavior because their conduction mechanism becomes quasi-one-dimensional which in turn results in an opening in their band-gap. Although there are several approaches to obtain GNRs, longitudinal unzipping of carbon nanotubes (CNTs) is one of the most common techniques to obtain semiconductive GNRs measuring a few nanometers in width (sGNRs)[8,9]. In our previous work, we successfully obtained single-layer sGNRs from single-walled[10-12] and double-walled[13-15] carbon nanotubes (SWNTs and DWNTs, respectively) by the unzipping method incorporating an ultrasonication process. Although sub-10 nm width sGNRs can be produced by the unzipping method and is suitable for mass production[16], its application in electronic devices to produce unzipped sGNRs is still limited. To the best of our knowledge, this is because there is no in-situ method to select only sGNRs from a mixture of unzipped sGNRs and CNTs.

One of the possible approaches to separate only sGNRs from CNTs is the dielectrophoresis (DEP) technique,[17-19] which is the method for nanomaterial alignment without any contamination. It is applied both in the alignment of nanowires from metal to insulate and in separating different electrical properties such as metal and semiconductive CNTs (mCNTs and sCNTs, respectively). The separation capability is owed to the different DEP forces generated from different conductivities and permittivities in each material[20-25]. These merits indicate that DEP has a great potential for solving both the separation problem between sGNRs and CNTs and the alignment problem between the electrodes by leveraging on the different responses of the DEP force.

Here, we fabricated sGNRs from SWNTs using the unzipping method. One of the possible methods for separating sGNRs from a mixture with SWNT residues is the DEP process. The separated sGNRs were bridged between the micro-gap electrodes during the DEP process.

The frequency dependence phenomenon was also checked by changing the frequency of the applied AC bias voltage between the micro-gap electrodes. We succeeded in bridging only sGNRs between electrodes at 13 MHz or higher AC bias voltage because the repulsive DEP force of the SWNTs becomes stronger than that of sGNRs at 13 MHz or higher AC bias voltage. This finding was supported by the structural evaluation of bridging SWNTs/sGNRs and theoretical calculation of the DEP process.

HipCo SWNTs (Nanointegris) were annealed at 200 °C for 20 h to remove amorphous carbon, and then acid-treated with HCl (11.65 M at 109 °C) to remove the catalyst metal and induce defects. The GNRs were synthesized by unzipping 0.01 mg of SWNTs using 3 mg poly [(m-phenylenevinylene)-co-(2,5-dioctoxy-p-phenylene-vinylene)] (PmPV; Sigma-Aldrich) in 10 mL dichloroethane solvent. The solution was bath sonicated for 50 min at 37 kHz and 600 W (SHARP UT-606) to initiate the unzipping process. Then, the solution was centrifuged for 16 h at 50,000 G (TOMY Suprema 23 High-Speed Centrifuge) to reduce the remaining SWNTs. The remaining solution (supernatant) was diluted with dichloroethane to reduce the concentration of the mixture SWNTs/GNRs in solution.

Micro-gap electrodes for DEP were fabricated by electron beam lithography (EBL) on a SiO_2 substrate. The residue solution (ZEP520A: anisole = 1:1) for EBL was spin-coated onto the substrate spinning at 3000 rpm for 60 s. Then, the substrate was pre-baked at 180 °C for 2 min. Electrode patterning was performed by EBL (Elionix ELS-7500) and subsequently developed with a ZED-50 N solution. Titanium and platinum (Ti/Pt) electrodes with a thickness of 6/24 nm were deposited on the patterned substrate by sputtering (Miller CFS-4EP-LL). The EBL residue was then removed by dimethyl sulfoxide at 80 °C. Subsequently, the substrate was cleaned with isopropanol and deionized (DI) water under sonication.

The solution of SWNTs/GNRs obtained above was cast around the Ti/Pt electrodes, followed by DEP. The Ti/Pt electrodes were conducted by applying an AC bias voltage for 2 min at different frequencies, ranging from 500 kHz to 15 MHz (33120A Hewlett Packard Function Generator), as shown in figure 1. Then, the DEP sample was cleaned with chloroform, dichloroethane, acetone, ethanol, and DI water in that order and subsequently annealed at 200 °C for 1.5 h to remove PmPV, dust, and to increase the adhesion between the GNRs and electrodes. The I-V characteristics of the fabricated samples were measured using a probe system (Pascal Co., Ltd) with a semiconductor parameter analyzer (Agilent

4156B). The fabricated sample was also measured by atomic force microscopy (AFM; JEOL JSPM-5200) and Raman spectroscopy (Nano Photon Raman Touch) with a 533 nm laser for sample evaluation.

Fig. 1

The AC frequency-dependent bridging results of DEP from the SWNT/GNR mixture were observed using AFM, as shown in Fig. 2, in which DEP was performed at (a) 500 kHz, (b) 5 MHz, (c) 10 MHz, and (d) 15 MHz, respectively, with 5 Vpp of an applied voltage by 2 μm gap electrodes. The number of bridged SWNT/sGNRs was estimated by the height of the AFM images between electrodes compared to AFM images of the height and width of single GNRs, which is approximately 0.6 nm and 3 nm, respectively. By increasing the frequency of the DEP, the number of bridged SWNT/sGNRs was reduced from approximately 6000 (500 kHz) or less than 2000 (5 MHz, 10 MHz) to less than 500 (15 MHz). Similar trends were also obtained by varying the applied voltage (1, 5, 10 V) and electrode (gap size to 2 μm).

Fig. 2

Confocal Raman microscopy was performed to confirm the type of nanowires bridged between the micro-gap electrodes. Here, possible nanowires were SWNTs and/or GNRs because the presence of D and G band peaks in the Raman spectrum indicate that nanocarbon materials, such as unzipped GNRs and SWNTs, were successfully bridged by DEP, as shown in Fig. 3. From the Raman spectra, GNRs and SWNTs can be distinguished by the presence of peaks from the radial breathing mode (RBM). RBM is generated from the stretching in the diameter direction, which means only SWNTs have this stretching mode. The inset in Fig. 3 shows the Raman spectra of the RBM in SiO_2 (substrate), pretreated SWNTs before unzipping, and bridging SWNTs/GNRs with AC bias frequency dependence, respectively. At first, the RBM peaks of pretreated SWNTs before unzipping appeared at approximately 200-300 cm^{-1}, which indicates that the SWNTs were composed only of metallic SWNTs (mSWNTs) by considering the Kataura-plot,[26,27] which suggests that only mSWNTs and sGNRs remained after the unzipping process. Below 12 MHz, the presence of RBM peaks showed that SWNT residue remains as bridged material by DEP. In contrast, RBM peaks were missing from the sample obtained at frequencies higher than 13 MHz, which indicated

that only GNRs can bridge between electrodes. It was proved that only GNRs were successfully separated from a mixture of GNRs with SWNT residue by DEP at frequencies higher than 13 MHz of AC bias.

Fig. 3

During the DEP, objects are polarized with an inhomogeneous external electric field. The polarized object generates a side force that moves the object toward higher or lower electric field regions. The DEP force depends on the electric properties of the object and mediums, object size and shape, and the frequency of the electric field. The force generated by an electric field $\boldsymbol{E}$ on a dipole with dipole moment $\boldsymbol{p}$ is given by

$$\boldsymbol{F} = (\boldsymbol{p} \cdot \boldsymbol{\nabla})\boldsymbol{E} \qquad . \tag{1}$$

In an AC electric field, the time-averaged force on the object is given by

$$\boldsymbol{F_{DEP}} = \boldsymbol{\Gamma} \cdot \boldsymbol{\varepsilon_m} \boldsymbol{Re}\{\boldsymbol{CM}\} \boldsymbol{\nabla E} \qquad , \tag{2}$$

where Γ is the geometry factor of objects, ε_m is the real part of the permittivity of the medium, and $Re\ \{CM\}$ is the real part of the Claussius-Mossoti factor, which depends on the complex permittivity and conductivity of the medium and the object. [24,28)] For objects elongated in one direction, such as an oblate ellipsoid, carbon nanotubes, and graphene nanoribbons, CM is given by

$$\boldsymbol{CM} = \frac{\boldsymbol{\varepsilon_p}^* - \boldsymbol{\varepsilon_m}^*}{\boldsymbol{\varepsilon_m}^*}, \qquad \boldsymbol{\varepsilon}^* = \boldsymbol{\varepsilon} - \boldsymbol{i}\frac{\boldsymbol{\sigma}}{\boldsymbol{\omega}} \qquad , \tag{3}$$

where the real part of the CM can be described as

$$\boldsymbol{Re}\ \{\boldsymbol{CM}\} = \frac{\boldsymbol{\omega^2}\left(\boldsymbol{\varepsilon_m}\boldsymbol{\varepsilon_p} - \boldsymbol{\varepsilon_p}^2\right) + \left(\boldsymbol{\sigma_m}\boldsymbol{\sigma_p} - \boldsymbol{\sigma_m}^2\right)}{\boldsymbol{\varepsilon_m}^2\boldsymbol{\omega^2} + \boldsymbol{\sigma_m}^2} \qquad , \tag{4}$$

From equations (2) and (4), the DEP force of the sample will vary with the AC frequency, as shown in Fig. 4. This change in DEP force shows the possibility of separating the excess SWNTs from GNRs to bridge the gap between the micro-gap electrodes.

Bridging by the DEP force will be frequency-dependent as the applied frequency will change the $Re\ \{CM\}$, as stated in equation (4). The influence of the conductivity and permittivity of the medium and object to $Re\ \{CM\}$ in the high- and low-frequency limits is given by

$$\boldsymbol{Re\{CM\}} = \begin{cases} \dfrac{\boldsymbol{\sigma_p - \sigma_m}}{\boldsymbol{\sigma_m}}, & \boldsymbol{\omega \to 0} \\ \dfrac{\boldsymbol{\varepsilon_p - \varepsilon_m}}{\boldsymbol{\varepsilon_m}}, & \boldsymbol{\omega \to \infty} \end{cases} . \qquad (\mathbf{5})$$

where σ_p, σ_m, ε_p, ε_m and are the conductivity of the solute and medium, and the permittivity of the solute and medium, respectively. These values are summarized in Table 1. From the calculation of the limiting value in equation (5), there is a crossing point of the frequency-dependent DEP force function from equation (2) when the negative DEP force of the mSWNTs exceeds that of sGNRs. The inset in Fig. 4 shows that this crossing point is at 34.7 MHz in the negative DEP force region, which indicates that the repulsive DEP force of mSWNTs becomes stronger than that of sGNRs above this frequency. This suggests that the amount of bridging sGNRs is larger than that of mSWNTs in the higher frequency region than the crossing point.

Fig. 4, Table 1

The phenomenon generated in the DEP was considered by comparing the experimental DEP results with the theoretical prediction mentioned earlier. In the lower frequency region, the conductivity of the object (mSWNTs) is higher than that of the medium, which causes the DEP force to be positive. This positive DEP force pushes the object toward high electric field regions or to the gap between electrodes, as shown in Fig. 2 (a), at 500 kHz. Increasing the applied frequency will increase the influence of the object and medium permittivity. The permittivity of the object was lower than that of the medium, which generated a weakened DEP force and the object was moved from high electric field regions to low electric field regions. As a result, as the frequency increases, the bridging object between the electrodes is reduced, as shown in the AFM image in Fig. 2. For frequencies of more than 13 MHz, the

strength of repulsive DEP force between SWNTs and GNRs was different and only GNRs were bridged. From the experimental results, the frequency of the actual crossing point is estimated to be approximately 13 MHz because only sGNRs appear at these frequencies. The deviation between the theoretical simulation occurs because the object shape used in the simulation is only elongated in one direction like an oblate ellipsoid, which can change the crossing point to a lower frequency owing to the shape of the GNR being striped with one atomic layer thickness. The order of the experimental value coincides with the calculation value, which suggests that the experiment and calculation are consistent with each other when it comes to generated forces.

The amount of bridging sGNRs was simply adjusted by changing the concentration of the mixture in the solvent and applied voltage bias. Fig. 5a shows the AFM image of the small number of bridging sGNRs at 15 an AC bias voltage DEP in the concentration of diluted 1.25 times from the frequency-dependent sample. The average height of the sGNRs was approximately 0.6 nm. Bridging sGNRs were confirmed by the Raman imaging spectrum, as shown in Fig. 5 b,c,d. The diameter of the isolated SWNTs is estimated by

$$\boldsymbol{d = \frac{248}{\nu_{RBM}}} \qquad (\mathbf{6})$$

where ν_{RBM} is the wavenumber of the Raman shift in the RBM region[29]. From the Raman spectrum, as shown in Fig. 4, the diameter was estimated to be approximately 0.9 nm. AFM image showed the height of bridging sGNRs is lower than SWNTs. As such, it was proved that a single atomic layer of GNR bridging can be obtained by DEP. These results can be implemented in future organic electronics, especially nanoscale wiring, to create a molecular circuit.

Fig. 5

In summary, we fabricated sGNRs from mSWNTs by the unzipping method and investigated the separation of sGNRs from a mixture of mSWNT residue by the DEP technique by changing the frequency of the applied AC bias voltage between the micro-gap electrodes. From the structural and electrical evaluation of bridging mSWNTs/sGNRs, we successfully obtained bridging sGNRs without mSWNTs between electrodes at 13 MHz or

higher AC bias voltage. Theoretical calculations suggest that the repulsive DEP force from the electrodes in the mSWNTs becomes stronger than that in the sGNRs at 10^7 Hz or more, which separates sGNRs between electrodes in this frequency region. The separation of single-molecular-level sGNRs from SWNTs is achieved via the DEP method. This is a promising discovery in the study of nanoscale material electronics application.

Acknowledgments

This work was financially supported by KAKENHI of Nos. 15H03531, 19K22114, and 19H02559. This work was partially supported by “Nanotechnology Platform Program (NPP)” (Molecule and Material Synthesis, Grants number: S-20-KU-0006, JPMXP09FF20YA0015) of the Ministry of Education, Culture, Sports, Science and Technology (MEXT), Japan, and was also technologically supported by Kyushu University and Kitakyushu Semiconductor Center under the NPP. This work was performed under the Cooperative Research Program of the "Network Joint Research Center for Materials and Devices" from MEXT, Japan. WWA thanks to the MEXT scholarship for international students.

References

1) R. Parthasarathy, X.-M. Lin and H. M. Jaeger, Phys. Rev. Lett. **87**, 186807 (2001).

2) C. W. Marquardt, S. Grunder, A. Błaszczyk, S. Dehm, F. Hennrich, H. V. Löhneysen, M. Mayor and R. Krupke, Nat. Nanotechnol. **5**, 863 (2010).

3) M. Ratner, Nat. Nanotechnol. **8**, 378 (2013).

4) E. Lörtscher, Nat. Nanotechnol. **8**, 381 (2013).

5) A. K. Geim and K. S. Novoselov, Nat. Mater. **6**, 183 (2007).

6) K. I. Bolotin, K. J. Sikes, Z. Jiang, M. Klima, G. Fudenberg, J. Hone, P. Kim and H. L. Stormer, Solid State Commun. **146**, 351 (2008).

7) M. Y. Han, B. Özyilmaz, Y. Zhang and P. Kim, Phys. Rev. Lett. **98**, 206805 (2007).

8) D. V. Kosynkin, A. L. Higginbotham, A. Sinitskii, J. R. Lomeda, A. Dimiev, B. K. Price and J. M. Tour, Nature **458**, 872 (2009).

9) D. Wei, L. Xie, K. K. Lee, Z. Hu, S. Tan, W. Chen, C. H. Sow, K. Chen, Y. Liu and A. T. S. Wee, Nat. Commun. **4**, 1374 (2013).

10) M. Fukumori, R. R. Pandey, T. Fujiwara, A. TermehYousefi, R. Negishi, Y. Kobayashi, H. Tanaka and T. Ogawa, Jpn. J. Appl. Phys. **56**, 06GG12 (2017).

11) H. Furuki, T. Fujiwara, A. TermehYousefi and H. Tanaka, in *Proceedings of the 2017 IEEE Regional Symposium on Micro and Nanoelectronics* (2017).

12) M. Fukumori, S. Hara, T. Ogawa and H. Tanaka, Jpn. J. Appl. Phys. **57**, 03ED01 (2018).

13) H. Tanaka, R. Arima, M. Fukumori, D. Tanaka, R. Negishi, Y. Kobayashi, S. Kasai, T. K. Yamada and T. Ogawa, Sci. Rep. **5**, 12341 (2015).

14) R. R. Pandey, M. Fukumori, A. Termehyousefi, M. Eguchi, D. Tanaka, T. Ogawa and H. Tanaka, Nanotechnology **28**, 175704 (2017).

15) T. K. Yamada, H. Fukuda, T. Fujiwara, P. Liu, K. Nakamura, S. Kasai, A. L. Vazquez De Parga and H. Tanaka, Nanotechnology **29**, 315705 (2018).

16) A. Narita, X. Feng, Y. Hernandez, S. A. Jensen, M. Bonn, H. Yang, I. A. Verzhbitskiy, C. Casiraghi, M. R. Hansen, A. H. R. Koch, G. Fytas, O. Ivasenko, B. Li, K. S. Mali, T. Balandina, S. Mahesh, S.

De Feyter and K. Müllen, Nat. Chem. **6**, 126 (2014).

17) J. Cao and A. M. Ionescu, in *Proceedings of the IEEE Conference on Nanotechnology* (2012).

18) M. V. P. dos Santos, F. Béron, K. R. Pirota, J. A. Diniz and S. Moshkalev, *Electrical Manipulation of a Single Nanowire by Dielectrophoresis* (2017).

19) S. Shekhar, P. Stokes and S. I. Khondaker, ACS Nano **5**, 1739 (2011).

20) J. J. Boote and S. D. Evans, Nanotechnology **16**, 1500 (2005).

21) S. Raychaudhuri, S. A. Dayeh, D. Wang and E. T. Yu, Nano Lett. **9**, 2260 (2009).

22) E. M. Freer, O. Grachev, X. Duan, S. Martin and D. P. Stumbo, Nat. Nanotechnol. **5**, 525 (2010).

23) M. V. Puydinger dos Santos, L. P. B. Lima, R. A. Mayer, F. Béron, K. R. Pirota and J. A. Diniz, J. Vac. Sci. Technol. B, Nanotechnol. Microelectron. Mater. Process. Meas. Phenom. **33**, 031804 (2015).

24) M. Dimaki and P. Bøggild, Nanotechnology **15**, 1095 (2004).

25) M. J. Mendes, H. K. Schmidt and M. Pasquali, J. Phys. Chem. B **112**, 7467 (2008).

26) H. Kataura, Y. Kumazawa, Y. Maniwa, I. Umezu, S. Suzuki, Y. Ohtsuka and Y. Achiba, Synth. Met. **103**, 2555 (1999).

27) Q. Cheng, S. Debnath, E. Gregan and H. J. Byrne, Appl. Phys. A Mater. Sci. Process. **102**, 309 (2011).

28) J. E. Kim and C. S. Han, Nanotechnology **16**, 2245 (2005).

29) A. Jorio, R. Saito, J. H. Hafner, C. M. Lieber, M. Hunter, T. McClure, G. Dresselhaus and M. S. Dresselhaus, Phys. Rev. Lett. **86**, 1118 (2001).

30) J. Fang, W. G. Vandenberghe and M. V. Fischetti, Phys. Rev. B **94**, 045318 (2016).

31) I. M. Smallwood, *Handbook of Organic Solvent Properties* (Butterworth-Heinemann, 1996).

Figure Captions

Fig. 1. Schematic image of setup in DEP.

Fig. 2. AFM image of trapped GNRs between 2 μm gap electrode by DEP with (a) 500 kHz, (b) 5 MHz, (c) 10 MHz, and (d) 15 MHz frequency and 5 Vpp applied voltage.

Fig. 3. Raman spectrum obtained from DEP sample fabricated by varying the frequency of electric field. Black line shows the Raman spectrum of SiO_2 substrate. Red line represents the pretreated SWNTs before unzipping. From peak positions of Raman shift, the starting material is composed only by mSWNTs. (Inset) Enlarged Raman spectrum obtained from samples fabricated in higher DEP frequency. In case of 11 and 12 MHz samples, there were peaks of radial breathing modes from mSWNTs indicated by black arrows.

Fig. 4. Semilogarithmic plot of frequency dependent DEP force calculation of mSWNTs and sGNRs obtained from equations (2) and (4). Electric field was set as constant for easy consideration. The inset shows the enlarged double logarithmic plot of frequency-dependent DEP force. Negative DEP force indicates repulsive force from electrode gap. The frequency value of crossing point was 34.7 MHz, which indicates that the repulsive force of mSWNTs becomes stronger than that of sGNRs.

Fig. 5. a. AFM image of a few sGNRs trapped between electrodes by DEP. The concentration of mixture after unzipping was lower than that of frequency-dependent sample. The height of individual wires is shown in inset. b, c, d**.** Raman imaging spectrum of a few bridging sGNRs in Fig. 5 a. Raman imaging at SiO_2 (Raman shift: 520 cm^{-1}, b) and G band (Raman shift: 1580 cm^{-1}, c) between electrodes. The gray scale shows the Raman intensity. The incident laser light was not completely irradiated to SiO_2 substrate in Pt electrode region, which occurs due to low Raman intensity at SiO_2 Raman imaging. d. Raman spectra from imaging in 8 pixel as shown in Fig.5 b,c. Owing to the presence of G band and absence of RBM as shown in the upper inset, these Raman spectra originated from sGNRs.

Table I. Electrical parameter of mSWNTs, sGNRs and dichloroethane. Limit value of DEP force from calculation is included.

Materials	Conductivity ($S \cdot m^{-1}$)	Permittivity ($F \cdot m^{-1}$)	$\frac{\sigma_p - \sigma_m}{\sigma_m}$	$\frac{\varepsilon_p - \varepsilon_m}{\varepsilon_m}$
mSWNTs	1.0×10^{8} (ref.[24])	-8.9×10^{-8} (ref.[24])	2.5×10^{18}	-9.6×10^{2}
sGNRs	3.7×10^{-11}	6.1×10^{-11} (ref. [30])	-7.5×10^{-2}	-3.4×10^{-1}
Dichloroethane	4.0×10^{-11} (ref.[31])	9.3×10^{-11} (ref.[31])	–	–

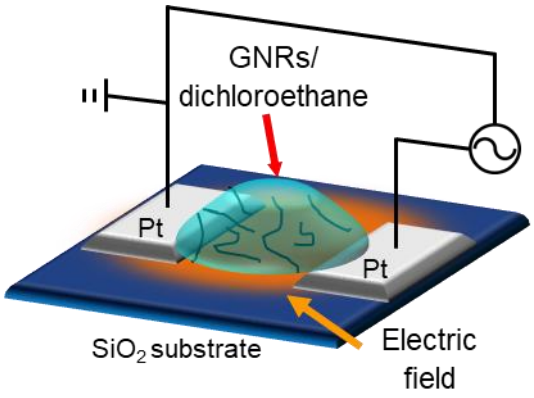

Figure 1.

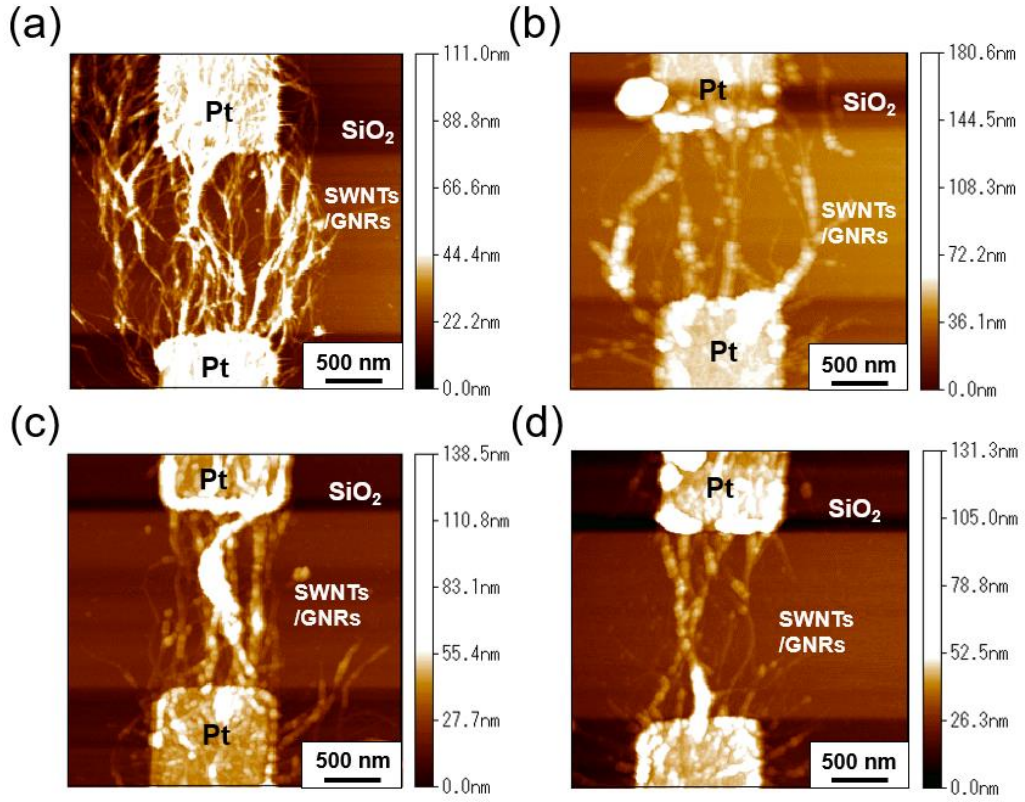
(a)
Pt
SiO2
SWNTs
/GNRs
Pt
500 nm
111.0nm
88.8nm
66.6nm
44.4nm
22.2nm
0.0nm
(b)
Pt
SiO2
SWNTs
/GNRs
Pt
500 nm
180.6nm
144.5nm
108.3nm
72.2nm
36.1nm
0.0nm
(c)
Pt
SiO2
SWNTs
/GNRs
Pt
500 nm
138.5nm
110.8nm
83.1nm
55.4nm
27.7nm
0.0nm
(d)
Pt
SiO2
SWNTs
/GNRs
500 nm
131.3nm
105.0nm
78.8nm
52.5nm
26.3nm
0.0nm

Figure 2.

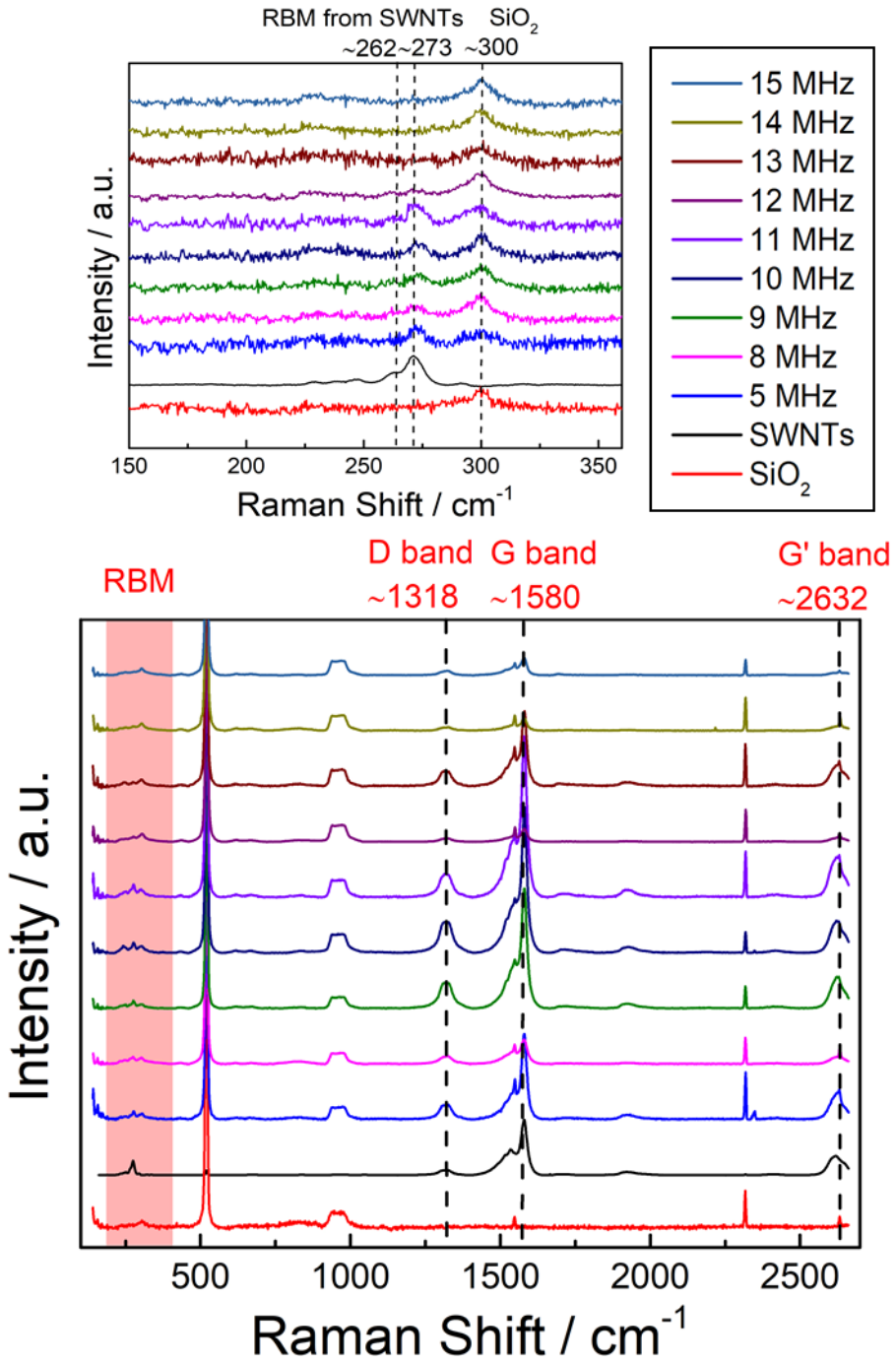
RBM from SWNTs
SiO2
~262~273
~300
Intensity / a.u.
150
200
250
300
350
Raman Shift / cm-1
15 MHz
14 MHz
13 MHz
12 MHz
11 MHz
10 MHz
9 MHz
8 MHz
5 MHz
SWNTs
SiO2
RBM
D band
~1318
G band
~1580
G' band
~2632
Intensity / a.u.
500
1000
1500
2000
2500
Raman Shift / cm-1

Figure 3.

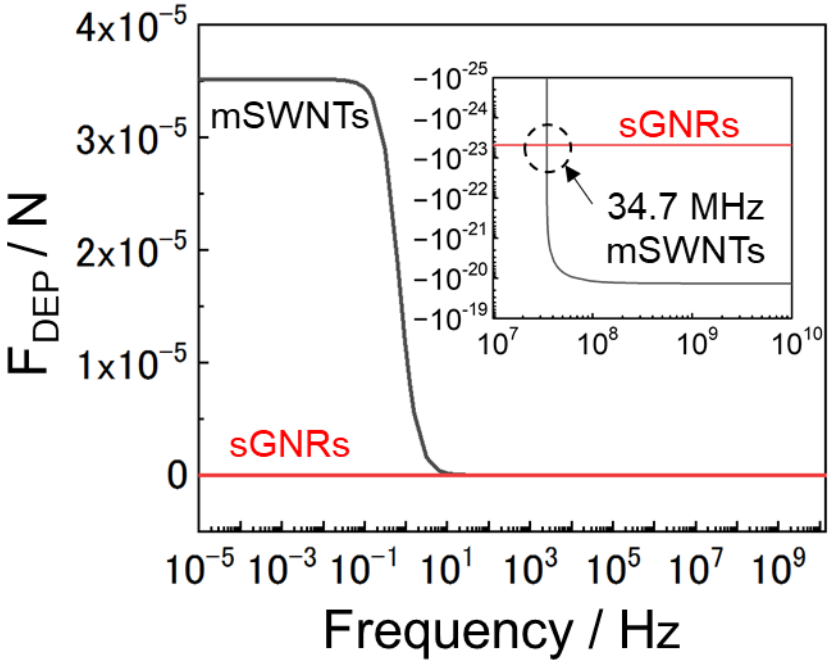
4x10⁻⁵
3x10⁻⁵
2x10⁻⁵
1x10⁻⁵
0
F_DEP / N
mSWNTs
sGNRs
10⁻⁵ 10⁻³ 10⁻¹ 10¹ 10³ 10⁵ 10⁷ 10⁹
Frequency / Hz
−10⁻²⁵
−10⁻²⁴
−10⁻²³
−10⁻²²
−10⁻²¹
−10⁻²⁰
−10⁻¹⁹
10⁷ 10⁸ 10⁹ 10¹⁰
sGNRs
34.7 MHz
mSWNTs

Figure 4.

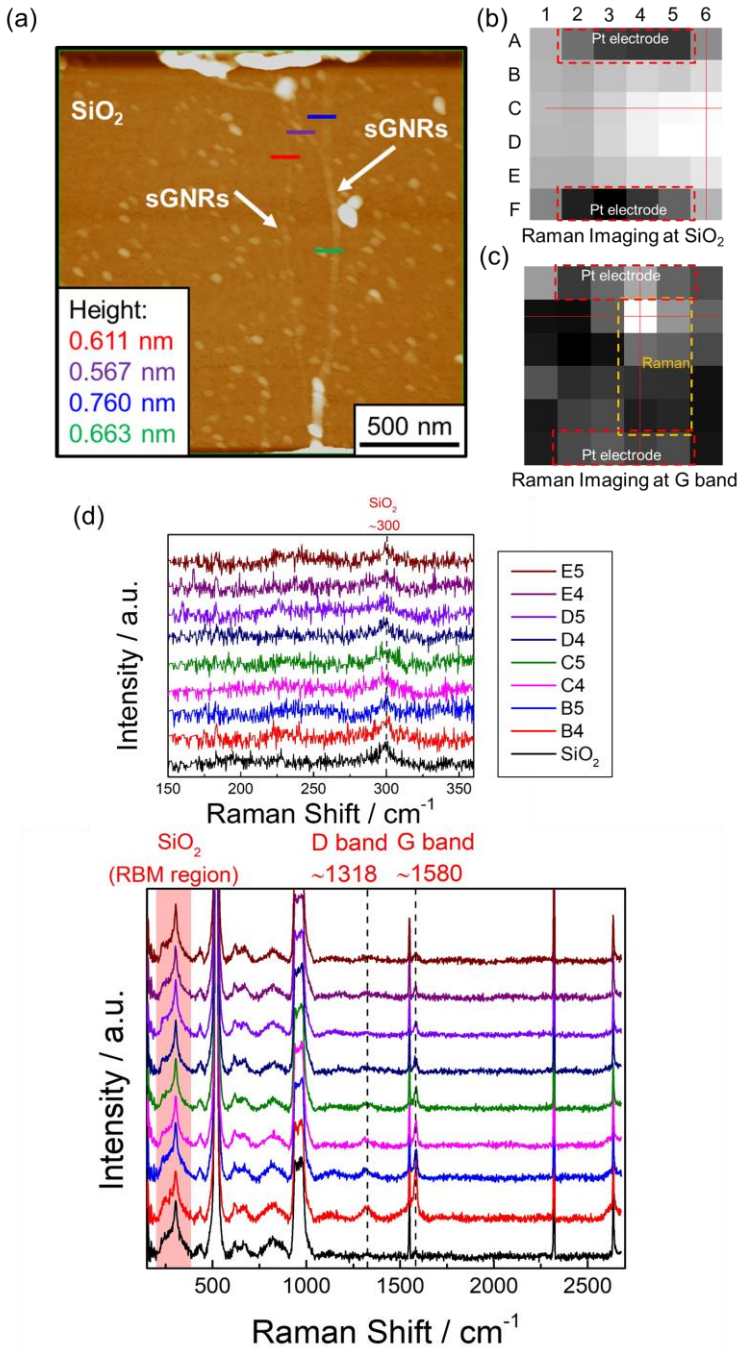
(a)
SiO2
sGNRs
sGNRs
Height:
0.611 nm
0.567 nm
0.760 nm
0.663 nm
500 nm
(b)
1 2 3 4 5 6
A
B
C
D
E
F
Pt electrode
Pt electrode
Raman Imaging at SiO2
(c)
Pt electrode
Raman
Pt electrode
Raman Imaging at G band
(d)
SiO2
~300
Intensity / a.u.
150 200 250 300 350
Raman Shift / cm-1
E5
E4
D5
D4
C5
C4
B5
B4
SiO2
SiO2
(RBM region)
D band G band
~1318 ~1580
Intensity / a.u.
500 1000 1500 2000 2500
Raman Shift / cm-1

Figure 5.

.